The Journal of Chemical Physics

Nuclear magnetic shielding of molecule in solution based on reference interaction site model self-consistent field with spatial electron density distribution

Cite as: J. Chem. Phys. **152**, 194102 (2020); https://doi.org/10.1063/5.0008903
Submitted: 26 March 2020 . Accepted: 27 April 2020 . Published Online: 18 May 2020

Kosuke Imamura, Takeshi Yamazaki, Daisuke Yokogawa, Masahiro Higashi, and Hirofumi Sato

The Journal of Chemical Physics ARTICLE scitation.org/journal/jcp

Nuclear magnetic shielding of molecule in solution based on reference interaction site model self-consistent field with spatial electron density distribution

Cite as: J. Chem. Phys. 152, 194102 (2020); doi: 10.1063/5.0008903
Submitted: 26 March 2020 • Accepted: 27 April 2020 •
Published Online: 18 May 2020

Kosuke Imamura,[1] Takeshi Yamazaki,[2] Daisuke Yokogawa,[3] Masahiro Higashi,[1,4] and Hirofumi Sato[1,4,5,a)]

AFFILIATIONS

[1] Department of Molecular Engineering, Graduate School of Engineering, Kyoto University, Kyoto 615-8510, Japan
[2] 1QB Information Technologies (1QBit), 200-1285 West Pender Street, Vancouver, British Columbia V6E 4B1, Canada
[3] Graduate School of Arts and Science, The University of Tokyo, Komaba, Meguro-ku, Tokyo 153-8902, Japan
[4] Elements Strategy Initiative for Catalysts and Batteries (ESICB), Kyoto University, Kyoto 615-8520, Japan
[5] Fukui Institute for Fundamental Chemistry, Kyoto University, Kyoto 606-8103, Japan

[a)] **Author to whom correspondence should be addressed:** hirofumi@moleng.kyoto-u.ac.jp

ABSTRACT

A new method for calculating nuclear magnetic shielding in solutions is developed based on the reference interaction site model self-consistent field (RISM-SCF) with spatial electron density distribution (SEDD). In RISM-SCF-SEDD, the electrostatic interaction between the solute and the solvent is described by considering the spread of electron to obtain more realistic electronic structure in solutions. It is thus expected to allow us to predict more quantitative chemical shifts of a wide variety of chemical species in solutions. In this study, the method is applied to a water molecule in water and is validated by examining the dependence of the solvent temperature and density on chemical shifts. The dependence of solvent species is also investigated, and more accurate results are obtained for polar solvents compared to the previous RISM-SCF study. Another application example of this method is the ^{15}N chemical shifts of two azines in water, which is difficult to predict with the polarizable continuum model (PCM). Our results are in good agreement with the previous quantum mechanical/molecular mechanics study and experimental results. It is also shown that our method gives more realistic results for methanol and acetone than the PCM.

I. INTRODUCTION

Nuclear magnetic resonance (NMR) spectroscopy is one of the most powerful and important techniques to know the detail of the molecular structure.[1–4] It has been widely used for structure determination of complex molecules such as natural products[5] and proteins[6] as well as simple and common molecules. The dynamic processes such as protein folding[7,8] and molecular self-assembly[9,10] have also been studied by tracing the time evolution of NMR spectra. In addition to experimental measurements, quantum chemical calculations have been performed to predict the magnetic properties of molecules, and their importance has been growing. There are many reports on the calculations with density functional theory (DFT), providing reasonable results to support experimental studies.[11–14] In terms of accuracy, the chemical shifts of heavy nuclei such as carbon, nitrogen, and fluorine in small molecules can be carried out within 1–2 ppm error from experimental results in the gas phase based on post Hartree–Fock (HF) methods, considering the vibrational effect at 0 K.[15] More recently, a quantitative prediction of NMR shieldings for organic molecules[16] and the calculation of NMR properties of liquid complex phases[17] were performed.

Considering that the majority of NMR measurements are performed in solution phases and solvent effects on NMR chemical shifts are large for some nuclei such as hydrogen, nitrogen, and oxygen, the methods taking the solvent effects into account are important when calculating nuclear magnetic shielding of a solvated molecule. As such, various methods have been developed so far, and they are roughly categorized into two groups: the implicit and explicit solvent models. One of the most popular and widely used methods of the implicit solvent models is the polarizable continuum model (PCM).[18,19] It has been shown that the modeling of solvent effects with the PCM generally leads to better results than the gas-phase calculation for the nucleus with a moderate interaction with solvents.[20,21] However, the specific effects such as hydrogen bonds and packing effect are not considered in the PCM although the electrostatic interactions with the surrounding solvent molecules are taken into account. Thus, several studies have observed that the calculated NMR chemical shifts of nuclei involved in hydrogen bond with solvent differ from experimental values when using only the PCM.[22–27] In order to describe such a system properly, the microscopic solvent structure in the first solvation shell is very important, namely, the specific interactions between the solute and solvents need to be described in an appropriate manner.[28] Therefore, explicit solvent models have often been used: the simplest example is the supermolecular or cluster model, where some solvent molecules are explicitly placed, and they are calculated with the same level of computation as the solute. There are a lot of studies with this model, indicating the improvement in the agreement with the experimental study compared to PCM results.[29–31] However, there are always problems on how to determine the number and position of solvent molecules. It is difficult to handle all solvent molecules with a fully quantum mechanical (QM) manner. Furthermore, even if the solvent positions are determined by structure optimization, it is not clear whether the configuration reflects the realistic solvation structure because the thermal effect is not considered here. One of the solutions to these problems is to generate multiple snapshots of configuration using molecular dynamics (MD) or Monte Carlo (MC) simulations, where the contribution from the solvent is treated by molecular mechanics (MM), i.e., QM/MM methods.[32] Several methods for NMR calculation with the QM/MM method have been developed,[33–39] and they have been applied to various systems.[26,27,40–44] However, it is still difficult to obtain statistically converged results (at least thousands of snapshots are needed) and to determine the QM region.[45]

Another approach to consider solvent effects in QM calculation is the reference interaction site model self-consistent field (RISM-SCF)[46,47] (see Refs. 48 and 49 for reviews). This is the combination of an *ab initio* electronic structure theory and an integral equation theory of molecular liquids based on statistical mechanics (RISM).[50,51] Here, the liquid structure of a solvent is described by intermolecular distribution functions between two atomic sites in solvent molecules, and the solute–solvent interaction is described with the distribution functions between solute and solvent sites. The electronic structure of the solute and the solute–solvent distribution functions are determined self-consistently, where the effects from the bulk solvent structure are efficiently taken into account. In addition, the method not only gives us direct access to statistically converged results but also allows us to examine the dependence of thermodynamic quantities such as temperature and density on various molecular properties derived by the electronic structure theory. Therefore, RISM-SCF has been widely utilized to study various chemical processes in solution.[48,52–56] The method of calculating the nuclear magnetic shielding tensor based on RISM-SCF was also developed where there is a little qualitative discussion.[57,58] In the original RISM-SCF method, the effective charges of the solute are determined by the least-squares fitting procedure to describe the electrostatic interaction between the solute and the solvent. However, this is troublesome in a sense that the charges depend on the choice of grid points, and the charges of buried sites are ill evaluated.[59] In addition, the spread of the electron distribution cannot be captured by the simple atomic charges.

Yokogawa *et al.* introduced auxiliary basis sets (ABSs) for fitting the electrostatic potential (ESP) with spatial electron density distribution (SEDD) to the original RISM-SCF.[60,61] This new generation of method, RISM-SCF-SEDD, does not require grid points for fitting ESP and gives more realistic picture of Coulomb interaction. Another advantage of RISM-SCF-SEDD is its high numerical stability, which enabled us to successfully apply the framework to more diverse systems.[62–68] Therefore, it is expected that the realistic description of the electrostatic interaction in RISM-SCF-SEDD has a potential to provide a better prediction of magnetic properties of the molecule in solution, but such a study has not yet been performed.

In this study, we develop a new method for calculating the nuclear magnetic shielding tensor based on the RISM-SCF-SEDD method. In Sec. II, the formulation of this method is shown. The application examples of this method are demonstrated in Sec. III. First, the chemical shifts of a water molecule in the solvent water are computed, and its temperature, density, and solvent dependence are examined. Then, the ^{15}N chemical shifts of two azines, which are typically mis-predicted with PCM,[24] are studied and compared to the previous QM/MM study.[44] The result indicates that our new method properly describes the electrostatic interaction and gives reasonable results compared to the QM/MM and experimental results for polar solvents.

II. THEORY

In order to remove the dependence of the gauge origin, we use gauge-invariant atomic orbitals (GIAOs).[69] A molecular orbital ψ_i is expanded with coefficients $C_{i\mu}$ and GIAOs χ_μ,

$$\psi_i = \sum_\mu C_{i\mu}(\mathbf{B},\mathbf{m})\chi_\mu(\mathbf{B}). \tag{1}$$

Here, we explicitly specify the dependence of the external magnetic field $\mathbf{B}$ and nuclear magnetic moments $\{\mathbf{m}\}$. Each GIAO centered on a nucleus M is expressed as

$$\chi_\mu(\mathbf{B}) = \exp\left(-\frac{i}{2}\mathbf{B}\times\mathbf{R}_{MO}\cdot\mathbf{r}\right)\phi_\mu, \tag{2}$$

where $\mathbf{R}_{MO}$ denotes the vector between the position of the nucleus M and an arbitrary gauge-origin O. With these GIAOs, we can define density matrix, one electron term, and two electron term as[58,70]

$$P_{\mu\nu}(\mathbf{B},\mathbf{m}) = 2\sum_i^{\mathrm{occ}} C^*_{i\mu}(\mathbf{B},\mathbf{m})C_{i\nu}(\mathbf{B},\mathbf{m}), \tag{3}$$

$$H_{\mu\nu}(\mathbf{B},\mathbf{m}) = \langle\chi_\mu|h(\mathbf{B},\mathbf{m})|\chi_\nu\rangle = \langle\phi_\mu|\exp\left(\tfrac{i}{2}\mathbf{B}\cdot\mathbf{R}_{MN}\times\mathbf{r}\right)h_N(\mathbf{B},\mathbf{m})|\phi_\nu\rangle, \quad (4)$$

$$G_{\mu\nu\rho\sigma}(\mathbf{B}) = \langle\chi_\mu\chi_\nu|r_{12}^{-1}|\chi_\rho\chi_\sigma\rangle = \langle\phi_\mu\phi_\nu|\exp\left\{\tfrac{i}{2}\mathbf{B}\cdot(\mathbf{R}_{MN}\times\mathbf{r}_1+\mathbf{R}_{RS}\times\mathbf{r}_2)\right\}r_{12}^{-1}|\phi_\rho\phi_\sigma\rangle. \quad (5)$$

The operator for one electron term is

$$h_N(\mathbf{B},\mathbf{m}) = \frac{1}{2}\left\{-i\nabla+\frac{1}{2}\mathbf{B}\times\mathbf{r}_N+\alpha_0^2\sum_K\frac{\mathbf{m}^K\times\mathbf{r}_K}{r_K^3}\right\}^2-\sum_K\frac{Z_K}{r_K}, \quad (6)$$

where $\mathbf{r}_K = \mathbf{r}-\mathbf{R}_K$ and α_0 is the fine structure constant.

In the RISM-SCF framework,[46,47] solvent distribution functions around a solute molecule are obtained by solving the RISM equation and hypernetted-chain (HNC) closure simultaneously,

$$h_{\gamma s}(r) = \sum_{\delta t}\omega_{\gamma\delta} * c_{\delta t} * \chi_{ts}(r), \quad (7)$$

$$h_{\gamma s}(r) = \exp[-\beta u_{\gamma s}(r)+h_{\gamma s}(r)-c_{\gamma s}(r)]-1, \quad (8)$$

where each Greek subscript corresponds to the solute sites, and roman one is of the solvent sites β is the inverse temperature defined by $\beta = \frac{1}{k_BT}$ with Boltzmann's constant k_B. $c_{\gamma s}$ is the direct correlation function, and $h_{\gamma s}$ is the total correlation function. ρ_s denotes the number density of the solvent site s. $\omega_{\gamma\delta}$ is the intramolecular correlation function, and χ_{ts} is defined as $\chi_{ts} = \omega_{ts}+\rho_t h_{ts}$. $u_{\gamma s}$ is the solute–solvent interaction function defined as the sum of Coulombic and Lennard-Jones (LJ) terms,

$$u_{\gamma s}(r) = u_{\gamma s}^{\mathrm{CL}}(r)+4\varepsilon_{\gamma s}\left\{\left(\frac{\sigma_{\gamma s}}{r}\right)^{12}-\left(\frac{\sigma_{\gamma s}}{r}\right)^{6}\right\}. \quad (9)$$

In RISM-SCF-SEDD,[60,61] auxiliary basis sets (ABSs) $\{f_i(\mathbf{r})\}$ are introduced,

$$f_i(\mathbf{r}) = C_i\exp\left(-\alpha_i|\mathbf{r}-\mathbf{R}_\gamma|^2\right) \qquad (i\in\gamma), \quad (10)$$

and its linear combination is fitted to the solute electron density

$$\tilde{\rho}(\mathbf{r}) = \sum_i^{N_{\mathrm{ABS}}} d_i f_i(\mathbf{r}) \to \sum_{\mu\nu}P_{\mu\nu}\phi_\mu(\mathbf{r})\phi_\nu(\mathbf{r}). \quad (11)$$

N_{ABS} is the number of ABSs, and constants C_i, α_i, and N_{abs} are defined as in the previous study.[60] The coefficients d_i are determined by[60]

$$\mathbf{d}(\mathbf{B},\mathbf{m}) = \mathbf{X}^{-1}\mathrm{tr}[\mathbf{PY}]-\frac{\mathbf{Z}^t\mathbf{X}^{-1}\mathrm{tr}[\mathbf{PY}]-N_e}{\mathbf{Z}^t\mathbf{X}^{-1}\mathbf{Z}}\mathbf{X}^{-1}\mathbf{Z}, \quad (12)$$

where

$$X_{ij} = \iint d\mathbf{r}_1 d\mathbf{r}_2\, f_i(\mathbf{r}_1)|\mathbf{r}_1-\mathbf{r}_2|f_j(\mathbf{r}_2), \quad (13)$$

$$Y_{\mu\nu,i}(\mathbf{B}) = \iint d\mathbf{r}_1 d\mathbf{r}_2\,\chi_\mu^*(\mathbf{r}_1)\chi_\nu(\mathbf{r}_1)|\mathbf{r}_1-\mathbf{r}_2|f_i(\mathbf{r}_2), \quad (14)$$

$$Z_i = \int d\mathbf{r}\, f_i(\mathbf{r}). \quad (15)$$

The introduction of ABSs changes the Coulombic interaction term in Eq. (9) from the classical form $(q_\gamma q_s/r)$ to

$$u_{\gamma s}^{\mathrm{CL}}(r) = -q_s\sum_{i\in\gamma}d_i\int d\mathbf{r}'\frac{f_i(\mathbf{r}')}{|\mathbf{r}-\mathbf{r}'|}+\frac{q_sZ_\gamma}{r}, \quad (16)$$

where q with subscripts is the partial charge of a solute site, and Z_γ is the nuclear charge of site γ.

We variationally minimize the Helmholtz free energy A defined as

$$A = E_{\mathrm{solute}}+\Delta\mu, \quad (17)$$

and obtain the solvated Fock matrix[60]

$$\mathbf{F}^{\mathrm{SEDD}} = \mathbf{F}^{\mathrm{gas}}-\mathbf{V}\mathbf{X}^{-1}\mathbf{Y}+\frac{\mathbf{V}\mathbf{X}^{-1}\mathbf{Z}}{\mathbf{Z}^t\mathbf{X}^{-1}\mathbf{Z}}[\mathbf{Z}^t\mathbf{X}^{-1}\mathbf{Y}-\mathbf{S}]. \quad (18)$$

Here, the gas-phase Fock matrix is introduced as $\mathbf{F}^{\mathrm{gas}} = \mathbf{H}+\mathrm{tr}[\mathbf{PG}]$. $\mathbf{V}$ is a row vector whose components are expressed as

$$V_i = \sum_s\rho_sq_s\int d\mathbf{r}\,h_{\gamma s}(|\mathbf{r}-\mathbf{R}_\gamma|)\int d\mathbf{r}'\frac{f_i(\mathbf{r}')}{|\mathbf{r}-\mathbf{r}'|} = \sum_s\rho_sq_sC_i\left(\frac{\pi}{\alpha_i}\right)^{3/2}\times\int_0^\infty dr\,4\pi r^2h_{\gamma s}(r)\frac{\mathrm{erf}(\sqrt{\alpha_i}r)}{r} \qquad (i\in\gamma). \quad (19)$$

E_{solute} is the electronic energy of the solute molecule given by

$$E_{\mathrm{solute}} = \sum_{\mu\nu}P_{\mu\nu}(\mathbf{B},\mathbf{m})\left\{H_{\mu\nu}(\mathbf{B},\mathbf{m})+\frac{1}{2}\sum_{\rho\sigma}P_{\rho\sigma}(\mathbf{B},\mathbf{m})G_{\mu\nu\rho\sigma}(\mathbf{B})\right\}. \quad (20)$$

$\Delta\mu$ is the excess chemical potential, and when using the HNC closure relation, the formalism is provided by[71]

$$\begin{aligned}\Delta\mu &= -\frac{1}{\beta}\sum_{\gamma s}\rho_s\int d\mathbf{r}\left[c_{\gamma s}(r)-\frac{1}{2}h_{\gamma s}^2(r)+\frac{1}{2}h_{\gamma s}(r)c_{\gamma s}(r)\right]\\ &= -\frac{1}{\beta}\sum_{\gamma s}\rho_s\int d\mathbf{r}\left[e^{-\beta u_{\gamma s}(r)+t_{\gamma s}(r)}-1-t_{\gamma s}(r)+\frac{1}{2}h_{\gamma s}^2(r)-h_{\gamma s}(r)t_{\gamma s}(r)\right]\\ &\quad+\frac{1}{(2\pi)^3\beta}\int d\mathbf{k}\left[\sum_{\gamma s}\rho_t\hat{h}_{\gamma s}(k)\hat{c}_{\gamma s}(k)-\frac{1}{2}\sum_{\gamma\delta st}\rho_s\hat{c}_{\gamma s}(k)\hat{c}_{\delta t}(k)\hat{\chi}_{st}(k)\hat{\omega}_{\gamma\delta}(k)\right],\end{aligned} \quad (21)$$

where $t_{\gamma s} = h_{\gamma s}-c_{\gamma s}$ and hat symbol means the function in reciprocal space.

The components of the nuclear magnetic shielding tensor of a nucleus X ($\boldsymbol{\sigma}^X$) are described as the second derivative of A,[57,58]

$$\sigma_{\alpha\beta}^X = \left.\frac{\partial^2A(\mathbf{B},\mathbf{m})}{\partial B_\alpha\partial m_\beta^X}\right|_{\mathbf{B}=\mathbf{0},\mathbf{m}=\mathbf{0}} \qquad (\alpha,\beta = x,y,z). \quad (22)$$

Now, we differentiate both sides of Eq. (17) with respect to m_β^X and obtain the following equation (see Appendix A):

$$\begin{aligned}\frac{\partial A}{\partial m_\beta^X} &= \frac{\partial E_{\text{solute}}}{\partial m_\beta^X} + \frac{\partial \Delta\mu}{\partial m_\beta^X} \\ &= \sum_{\mu\nu}\frac{\partial P_{\mu\nu}}{\partial m_\beta^X}\left(H_{\mu\nu} + \sum_{\rho\sigma}P_{\rho\sigma}G_{\mu\nu\rho\sigma}\right) + \sum_{\mu\nu}P_{\mu\nu}\frac{\partial H_{\mu\nu}}{\partial m_\beta^X} \\ &\quad + \sum_{\gamma s}\rho_s\int d\mathbf{r}\, g_{\gamma s}(r)\left(-q_s\sum_{i\in\gamma}\frac{\partial d_i}{\partial m_\beta^X}\int d\mathbf{r}'\,\frac{f_i(\mathbf{r}')}{|\mathbf{r}-\mathbf{r}'|}\right) \\ &= \sum_{\mu\nu}\frac{\partial P_{\mu\nu}}{\partial m_\beta^X}F_{\mu\nu}^{\text{gas}} + \sum_{\mu\nu}P_{\mu\nu}\frac{\partial H_{\mu\nu}}{\partial m_\beta^X} \\ &\quad - \sum_i\sum_s\rho_s q_s\int d\mathbf{r}\,\{h_{\gamma s}(r)+1\}\int d\mathbf{r}'\,\frac{f_i(\mathbf{r}')}{|\mathbf{r}-\mathbf{r}'|}\frac{\partial d_i}{\partial m_\beta^X} \\ &= \sum_{\mu\nu}\frac{\partial P_{\mu\nu}}{\partial m_\beta^X}F_{\mu\nu}^{\text{gas}} + \sum_{\mu\nu}P_{\mu\nu}\frac{\partial H_{\mu\nu}}{\partial m_\beta^X} - \sum_i V_i\frac{\partial d_i}{\partial m_\beta^X}. \end{aligned} \tag{23}$$

The last term of Eq. (23) does not appear in the original RISM-SCF study,[58] and this is expressed as follows:

$$\begin{aligned}\sum_i V_i\frac{\partial d_i}{\partial m_\beta^X} &= \sum_{\mu\nu}\frac{\partial P_{\mu\nu}}{\partial m_\beta^X}\sum_{ik}V_i X_{ik}^{-1}Y_{\mu\nu,k} - \frac{1}{\mathbf{Z}^t\mathbf{X}^{-1}\mathbf{Z}} \\ &\quad\times\left(\sum_{im}V_i X_{im}^{-1}Z_m\right)\sum_{\mu\nu}\frac{\partial P_{\mu\nu}}{\partial m_\beta^X}\left\{\sum_{kl}Z_k X_{kl}^{-1}Y_{\mu\nu,l} - S_{\mu\nu}\right\} \\ &= \sum_{\mu\nu}\frac{\partial P_{\mu\nu}}{\partial m_\beta^X}\left\{\left(\mathbf{V}\mathbf{X}^{-1}\mathbf{Y}\right) - \frac{\mathbf{V}\mathbf{X}^{-1}\mathbf{Z}}{\mathbf{Z}^t\mathbf{X}^{-1}\mathbf{Z}}\left(\mathbf{Z}^t\mathbf{X}\mathbf{Y}-\mathbf{S}\right)\right\}_{\mu\nu}. \end{aligned} \tag{24}$$

We insert Eq. (24) into Eq. (23) and obtain the following equation:

$$\begin{aligned}\frac{\partial A}{\partial m_\beta^X} &= \sum_{\mu\nu}\frac{\partial P_{\mu\nu}}{\partial m_\beta^X}\left(\mathbf{F}^{\text{gas}} - \mathbf{V}\mathbf{X}^{-1}\mathbf{Y} + \frac{\mathbf{V}\mathbf{X}^{-1}\mathbf{Z}}{\mathbf{Z}^t\mathbf{X}^{-1}\mathbf{Z}}\left(\mathbf{Z}^t\mathbf{X}\mathbf{Y}-\mathbf{S}\right)\right)_{\mu\nu} \\ &\quad + \sum_{\mu\nu}P_{\mu\nu}\frac{\partial H_{\mu\nu}}{\partial m_\beta^X} \\ &= \sum_{\mu\nu}\frac{\partial P_{\mu\nu}}{\partial m_\beta^X}F_{\mu\nu}^{\text{SEDD}} + \sum_{\mu\nu}P_{\mu\nu}\frac{\partial H_{\mu\nu}}{\partial m_\beta^X}. \end{aligned} \tag{25}$$

It is noted that the first-order differentiation of the density matrix with respect to m_β^X is skew-symmetric. The trace of the product of a symmetric and a skew-symmetric matrix is zero, and this concludes that

$$\left.\frac{\partial A}{\partial m_\beta^X}\right|_{\mathbf{m}=\mathbf{0}} = \sum_{\mu\nu}P_{\mu\nu}^{(0)}(H_{\mu\nu}^{(0,1)})_\beta^X, \tag{26}$$

where Ditchfield's notation is utilized.[69]

The nuclear magnetic shielding tensor is now expressed as the derivative of Eq. (26) with respect to B_α,

$$\sigma_{\alpha\beta}^X = \sum_{\mu\nu}\left\{P_{\mu\nu}^{(0)}(H_{\mu\nu}^{(1,1)})_{\alpha\beta}^X + (P_{\mu\nu}^{(1,0)})_\alpha(H_{\mu\nu}^{(0,1)})_\beta^X\right\}. \tag{27}$$

In order to obtain $(P_{\mu\nu}^{(1,0)})_\alpha$, the coupled perturbed Hartree–Fock equation needs to be solved. The first derivative of the solvated Fock matrix with respect to B_α at zero field is

$$\begin{aligned}(F_{\mu\nu}^{(1,0)})_\alpha &= (H_{\mu\nu}^{(1,0)})_\alpha + \sum_{\rho\sigma}P_{\rho\sigma}^{(0)}(G_{\mu\nu\rho\sigma}^{(1,0)})_\alpha \\ &\quad + \sum_{\rho\sigma}(P_{\rho\sigma}^{(1,0)})_\alpha G_{\mu\nu\rho\sigma}^{(0)} - \left(\mathbf{V}\mathbf{X}^{-1}(\mathbf{Y}^{(1,0)})_\alpha\right)_{\mu\nu} \\ &\quad + \frac{\mathbf{V}\mathbf{X}^{-1}\mathbf{Z}}{\mathbf{Z}^t\mathbf{X}^{-1}\mathbf{Z}}\left\{\mathbf{Z}^t\mathbf{X}^{-1}(\mathbf{Y}^{(1,0)})_\alpha - (\mathbf{S}^{(1,0)})_\alpha\right\}_{\mu\nu}, \end{aligned} \tag{28}$$

where

$$(S_{\mu\nu}^{(1,0)})_\alpha = \langle\tfrac{i}{2}(\mathbf{R}_{MN}\times\mathbf{r})_\alpha\phi_\mu|\phi_\nu\rangle, \tag{29}$$

$$(Y_{\mu\nu,i}^{(1,0)})_\alpha = \langle\tfrac{i}{2}(\mathbf{R}_{MN}\times\mathbf{r}_1)_\alpha\phi_\mu(\mathbf{r}_1)\phi_\nu(\mathbf{r}_1)|\,|\mathbf{r}_1-\mathbf{r}_2|\,|f_i(\mathbf{r}_2)\rangle. \tag{30}$$

It is noted that the derivative of V_i with respect to B_α at zero field vanishes (see Appendix B),

$$\left.\frac{\partial V_i}{\partial B_\alpha}\right|_{\mathbf{B}=\mathbf{0}} = (V_i^{(1,0)})_\alpha = 0. \tag{31}$$

We introduce simple notation for $\phi_\mu(\mathbf{r})$ and $Y_{\mu\nu,i}$,

$$\begin{aligned}|\mathbf{m}) &= |m_x, m_y, m_z) \equiv \phi_\mu(\mathbf{r}) \\ &= (x-X_M)^{m_x}(y-Y_M)^{m_y}(z-Z_M)^{m_z}e^{-\alpha_M|\mathbf{r}-\mathbf{R}_M|^2}, \end{aligned} \tag{32}$$

$$(\mathbf{mn}|\mathbf{0}_i) \equiv Y_{\mu\nu,i}. \tag{33}$$

The x component of Eq. (30) is thus expressed as

$$\begin{aligned}(Y_{\mu\nu,i}^{(1,0)})_x &= \iint d\mathbf{r}_1 d\mathbf{r}_2\,\frac{i}{2}\{(\mathbf{R}_{MN})_y z_1 - (\mathbf{R}_{MN})_z y_1\} \\ &\quad\times\phi_\mu(\mathbf{r}_1)\phi_\nu(\mathbf{r}_1)|\mathbf{r}_1-\mathbf{r}_2|f_i(\mathbf{r}_2) \\ &= \frac{i}{2}\{Y_{MN}(z\mathbf{mn}|\mathbf{0}_i) - Z_{MN}(y\mathbf{mn}|\mathbf{0}_i)\} \\ &= \frac{i}{2}[Y_{MN}\{(\mathbf{m}+\mathbf{1}_z\mathbf{n}|\mathbf{0}_i) + Z_M(\mathbf{mn}|\mathbf{0}_i)\} \\ &\quad - Z_{MN}\{(\mathbf{m}+\mathbf{1}_y\mathbf{n}|\mathbf{0}_i) + Y_M(\mathbf{mn}|\mathbf{0}_i)\}], \end{aligned} \tag{34}$$

where $\mathbf{1}_\alpha = (\delta_{x\alpha}, \delta_{y\alpha}, \delta_{z\alpha})$. We can compute $(\mathbf{m}+\mathbf{1}_\alpha\mathbf{n}|\mathbf{0}_i)$ and $(\mathbf{mn}|\mathbf{0}_i)$ by recursion relations shown in the previous study.[72]

III. RESULTS AND DISCUSSION

All quantum chemical calculations were performed with Gaussian 16.[73] The program of the RISM-SCF-SEDD method and NMR calculation was incorporated by us. All the calculations including the gas-phase and PCM calculations were performed with 6D and 10F option due to the implementation of evaluating Eqs. (13), (14), and (30). The detail of the basis sets used in the study is described below. The convergence criteria of SCF and optimization were set to a tight level. For the DFT calculation, ultrafine grid was utilized.

The parameters for various solvents are shown in Tables I and II. The mixing rule of LJ parameters between different atoms was given by $\sigma_{ij} = (\sigma_i + \sigma_j)/2$ and $\varepsilon_{ij} = \sqrt{\varepsilon_i\varepsilon_j}$. The number densities of water, methanol, acetone, chloroform, and carbon tetrachloride are 0.033 36, 0.014 87, 0.008 187, 0.007 480, and 0.006 328 molecules/Å^3, respectively.

TABLE I. Coulomb and LJ parameters for solvents.

Solvent	Atom	q (e)	σ (Å)	ε (kcal/mol)
Water[a]	O	−0.820	3.166	0.1550
	H	0.410	1.000[b]	0.0560[b]
Methanol[c]	C	0.145	3.500	0.0660
	O	−0.683	3.120	0.1700
	HO	0.418	1.000[d]	0.0560[d]
	HC	0.040	2.500	0.0300
Acetone[e]	C	0.300	3.750	0.1050
	O	−0.424	2.960	0.2100
	Me	0.062	3.910	0.1600
$CHCl_3$[c]	C	0.179	3.400	0.1017
	H	0.082	2.200	0.0199
	Cl	−0.087	3.440	0.2993
CCl_4[c]	C	0.248	3.800	0.0500
	Cl	−0.062	3.470	0.2660

[a]SPC model.
[b]See Ref. 46.
[c]OPLS-AA.
[d]The LJ parameters of hydrogen are taken from the SPC parameters.
[e]OPLS-UA.

TABLE II. Geometrical parameters for solvents.

Solvent	Bond length (Å)		Angle (deg)	
Water[a]	r(O−H)	1.0000	θ(H−O−H)	109.47
Methanol[b]	r(O−H_O)	0.9450	θ(H_O−O−C)	108.50
	r(C-H_C)	1.0900	θ(O-C-H_C)	109.50
	r(C−O)	1.4100		
Acetone	r(C−Me)	1.5070	θ(Me−C−Me)	117.20
	r(C=O)	1.2220		
$CHCl_3$	r(C−H)	1.1000	θ(Cl−C−Cl))	111.30
	r(C−Cl)	1.7580		
CCl_4	r(C−Cl)	1.7690	θ(Cl−C−Cl)	109.47

[a]SPC model.
[b]One of the dihedral angles χ(H_C−C−O−H_O) is 180°.

A. H_2O in water

In order to test our method, we applied this method to H_2O in water and calculated the effect of the solvent temperature and density on chemical shifts. To compare with the results of the conventional RISM-SCF method, all parameters of H_2O were set the same as those in the previous study.[57] The HF method with the 6-311G** basis set was employed under the temperature at 298.15 K, 373.15 K, 473.15 K, 573.15 K, and 673.15 K. The value of 0.02002 molecules/Å^3 (0.6 g/cm^3) was used for the low-density condition.

Figures. 1(a) and 1(b) show the chemical shifts of the oxygen and hydrogen atoms due to the solvation effect ($\Delta\sigma_X = \sigma_X^{gas} - \sigma_X^{SEDD}$, where X = H or O) in various temperature and density conditions. It can be seen that the absolute value of each chemical shift decreases when the temperature is increased. It is also confirmed that the absolute values of chemical shifts are small under low density. These results are consistent with the physical intuition that the behavior at the high temperature and/or low density approaches to those in the gas phase. The obtained results about proton chemical shifts are in accord with the previous study.[57]

In Fig. 1(c), the sum of Mulliken charge of the two hydrogen atoms is plotted with respect to temperature. The Mulliken charge was adopted because it was employed in the previous work. Note that the sum of the nucleus and electron charge (charge density) was used in Ref. 57. It is observed that the charge becomes smaller at high temperature and close to the value in the gas phase. It is believed that the decrease was caused by the weakening of hydrogen bonding. This result is also consistent with the previous study.[57] The change in dipole moment of H_2O is also displayed in Fig. 1(d). The effects of temperature and density to dipole moment are in agreement with those of the Mulliken charge. This shows that the solvation promotes the polarization of H_2O.

B. H_2O in various solvents

Next, the method was applied to a variety of solvent systems. The chemical shifts of water molecule in various solvents and their temperature dependences were studied experimentally.[74] These results were investigated by the original RISM-SCF method,[58] but the values of chemical shifts were generally shifted toward higher magnetic field than experimental values. As such, we examined the proton chemical shifts of H_2O in water, acetone, chloroform, and carbon tetrachloride by this method. The calculations were performed with DFT using the B3LYP functional. Each solvent geometry was set to as in Table II. The geometries of H_2O and tetramethylsilane (TMS) were determined by structure optimization with the cc-pVTZ basis set. In the RISM-SCF-SEDD calculation, the same basis set is utilized, and the temperature was changed by 10 K from 283.15 K to 323.15 K. The solute LJ parameters used here were listed in Table III. In the original water models such as SPC[75] and TIP3P,[76] the LJ parameters were only assigned on the oxygen atom. Since the integral equation theory employs integration over the complete space, we need to put them on hydrogen atoms too.[77] Several parameters for hydrogen have been proposed,[78,79] and here, the values proposed by Pettitt and Rossky[79] (σ = 0.4 Å, ε = 0.046 kcal/mol) are utilized. We define a new parameter set by combining the SPC oxygen parameters with the hydrogen parameters. The LJ parameters of TMS were obtained from OPLS-AA.[80]

The values of ^{1}H nuclear magnetic shielding calculated by the above conditions are shown in Table IV. In terms of H_2O, it is found that the values in water and acetone are smaller than those in chloroform and carbon tetrachloride. It is considered that the effect of polar solvents to the electronic structure is larger than that of non-polar solvents. This tendency can be seen in the temperature dependence, namely, the temperature dependence in non-polar solvents is negligibly small. For TMS, we can see that the shielding did not change by the temperature difference. This is qualitatively consistent with an experimental study,[81] and it is believed that the appropriate description of TMS in solutions is achieved. The shielding also did not vary even if we changed solvents.

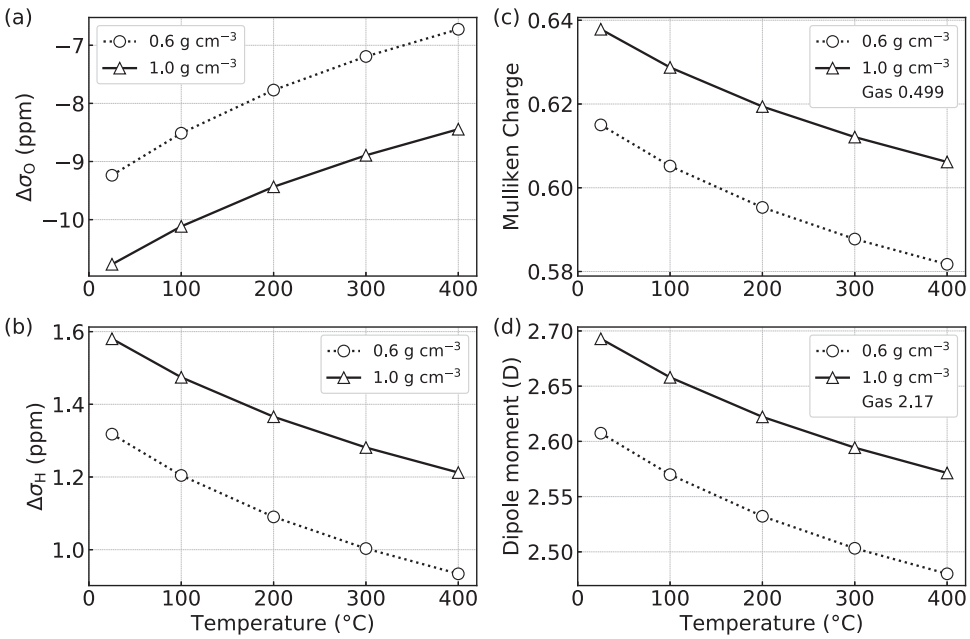

FIG. 1. [(a) and (b)] The chemical shifts of oxygen and hydrogen of H_2O plotted against the temperature and density of solvent. (c) The sum of the Mulliken charge of two hydrogen atoms and (d) the dipole moment of H_2O along the solvent temperature. Dotted lines are obtained at the low-density condition.

TABLE III. LJ parameter sets for solutes H_2O, TMS, and two azines.

Molecule	Atom	σ (Å)	ε (kcal/mol)
H_2O	O	3.160	0.1550
	H	0.400	0.0460
TMS[a]	Si	4.000	0.1000
	C	3.500	0.0660
	H	2.500	0.0300
Pyridazine, pyrazine[a]	N	3.250	0.1700
	C	3.550	0.0700
	H	2.420	0.0300

[a]OPLS-AA.

TABLE IV. The isotropic magnetic shielding of ^{1}H (ppm) obtained by the RISM-SCF-SEDD calculation at various temperatures. Four types of solvents such as water, acetone, chloroform, and carbon tetrachloride were utilized.

Solvent	Solute	10 °C	20 °C	30 °C	40 °C	50 °C
Water	H_2O	27.82	27.90	27.97	28.03	28.10
	TMS	31.69	31.69	31.69	31.69	31.69
Acetone	H_2O	29.45	29.53	29.61	29.68	29.75
	TMS	31.75	31.75	31.75	31.75	31.75
$CHCl_3$	H_2O	31.15	31.16	31.16	31.16	31.17
	TMS	31.74	31.74	31.74	31.74	31.74
CCl_4	H_2O	31.29	31.29	31.29	31.29	31.29
	TMS	31.74	31.74	31.74	31.74	31.74

We show the chemical shifts of H_2O in Fig. 2 calculated by subtracting the shielding of H_2O from that of TMS. We see that the order of chemical shifts is water > acetone > chloroform > carbon tetrachloride at any temperature. In addition, the slope of chemical shifts vs temperature is negative. This is consistent with the previous study of the conventional RISM-SCF method[58] and experimental data.[74] The chemical shifts in water and acetone become larger and more accurate compared to the previous study.[58] However, the shifts in chloroform and carbon tetrachloride were almost unchanged, and the values were underestimated compared to the experimental results. Note that the choice of hydrogen parameters (σ and ε) affects the solute electronic structure and solute–solvent distribution functions, and thus, the chemical shifts change. A careful consideration may be needed to obtain a realistic value of chemical shifts in polar solvents.

C. Pyridazine and pyrazine

Our next target molecules were two azines, pyridazine and pyrazine. ^{15}N chemical shifts are sensitive to the solvent, and the PCM method presented a difficulty in describing the solvation effect of polar solvents.[24] To overcome this, the model calculation in which solvent molecules were explicitly placed around a solute molecule was performed,[29] and the modified method of the PCM was developed.[44] In Ref. 44, the QM/MM calculation was also carried out to compare the results. We used this QM/MM result and experimental values for comparison in the following discussion.

In this section, all calculations were performed by the DFT method using the B3LYP functional. The optimized structures of the two molecules were obtained with the cc-pVTZ basis. LJ parameters for pyridazine and pyrazine were taken from the OPLS-AA force field.[82] As a comparison, the calculations with the integral equation formalism PCM (IEF-PCM)[83] were carried out. First, we

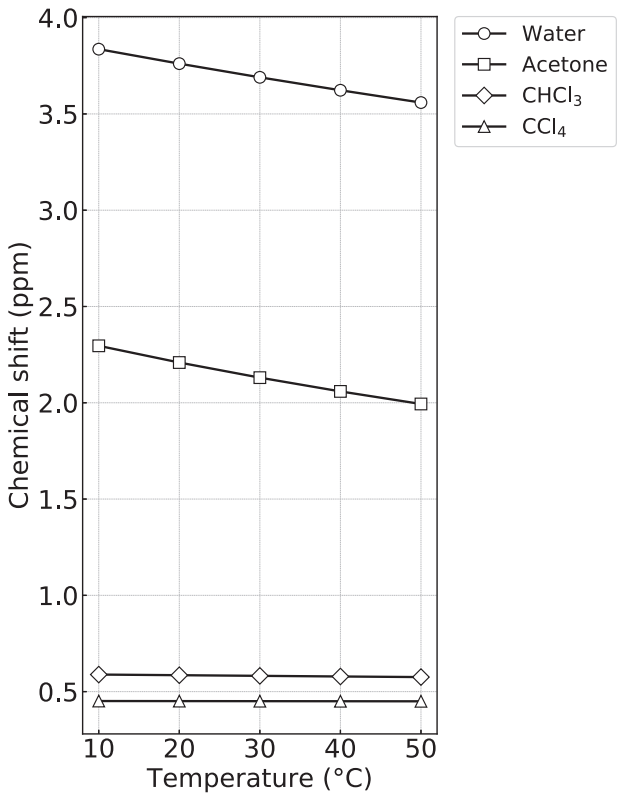

FIG. 2. The proton chemical shifts of H_2O relative to TMS in various solvents and its temperature dependence.

examined the basis set dependence on ^{15}N chemical shifts in water. We used three basis sets 6-31G**, 6-311G**, and cc-pVTZ. In each of the basis sets, the RISM-SCF-SEDD calculation was performed at 298.15 K. In Table V, the nuclear magnetic shielding of the nitrogen atom of the two azines and its chemical shift relative to the gas-phase shielding is shown. The dipole moment was also displayed in regard to pyridazine. As a comparison, the QM/MM result of Manzoni *et al.* and experimental values were displayed at the bottom of the table. It can be seen that the shift calculated by RISM-SCF-SEDD with the cc-pVTZ basis set is in very good agreement with the QM/MM and experimental results for both molecules. The advantage of our method is that we directly obtain statistically converged results at one calculation without explicitly sampling of solvent distributions, which is similar to the ASEC procedure[44] where only one quantum mechanical calculation is required.

When the size of basis sets gets larger, it is found that the chemical shifts become close to experimental values. The PCM results are insensitive to the basis set. The dipole moment of pyridazine is also in good agreement with the QM/MM result, where the value was systematically improved by using larger basis sets.

The radial distribution functions (RDFs) between a nitrogen atom on pyridazine and atoms on solvent water derived by the SEDD calculation with cc-pVTZ are shown in Fig. 3(a) with solid curves. The RDFs of the same atom pair were obtained in the previous QM/MM study,[44] which were digitalized using WebPlotDigitalizer[84] and shown in dashed curves. Regarding the NH pair (shown in red), we can see that the first peak position and height of the solid curve are in good agreement with the QM/MM result. This means that the proper description of the NH interaction is achieved, and its effect is reflected in the chemical shifts. The first peak of the NO pair is seen in the near region of that of the QM/MM result, but

TABLE V. The ^{15}N isotropic magnetic shielding and chemical shift with regard to the gas-phase value of pyridazine and pyrazine. Three basis sets were utilized, and the results were compared with the QM/MM results and experimental values.[44] The dipole moment of pyridazine was also shown.

		Pyridazine			Pyrazine	
Basis	Model	Shielding (ppm)	Shift (ppm)	Dipole (D)	Shielding (ppm)	Shift (ppm)
6-31G**	Gas	−167.5		4.09	−77.2	
	PCM	−143.1	24.4	5.29	−68.6	8.6
	SEDD	−124.0	43.5	6.13	−60.2	17.0
6-311G**	Gas	−217.9		4.16	−118.4	
	PCM	−190.3	27.6	5.43	−108.7	9.7
	SEDD	−167.4	50.5	6.36	−98.4	20.0
cc-pVTZ	Gas	−219.1		4.14	−121.5	
	PCM	−191.2	27.9	5.51	−111.7	9.8
	SEDD	−164.6	54.5	6.66	−99.7	21.8
I-QM/MM[a]			52.4	6.74		20.1
Experimental values[a]			42–54			17–22

[a]See Ref. 44.

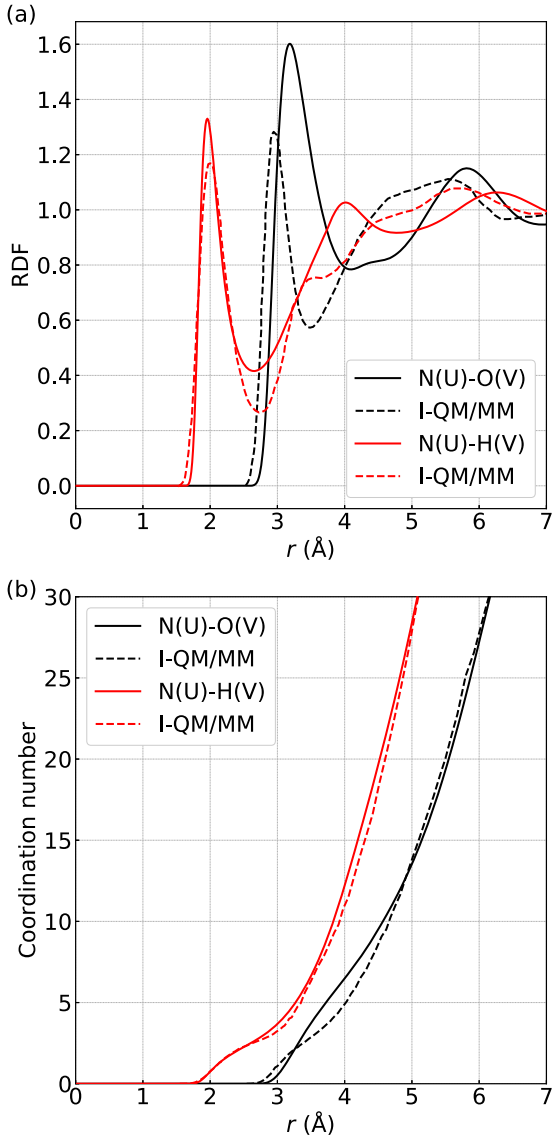

FIG. 3. (a) The RDFs between a nitrogen atom on solute (U) pyridazine and atoms on solvent (V) water. The red curves correspond to the N(U)-H(V) pair, and black ones are of the N(U)-O(V) pair. The results obtained by RISM-SCF-SEDD are shown in solid lines. RDFs of the same pair were obtained by the QM/MM calculation (dashed lines).[44] (b) Coordination numbers calculated by using Eq. (35). The curve type is the same as Fig. 3(a). The dashed curves are calculated using the QM/MM RDFs traced from Ref. 44.

the peak position is slightly shifted to the right. This implies that the angle N(U)-H(V)-O(V) is somewhat large, and the description of the second solvation shell in SEDD is not so good due to this. Nevertheless, it is assumed that the large portion of the electrostatic interaction can be properly considered because the dominant interaction lies between nitrogen and hydrogen. In order to compare the spatial distribution of water, the coordination numbers $N_X(r)$ at a distance r are shown in Fig. 3(b), which are calculated by using the following equation:

$$N_X(r) = 4\pi\rho_X \int_0^r dr'\, r'^2 g_X(r') \quad (X = O,H). \tag{35}$$

ρ_X is the number density of atom X in solvent water, and $g_X(r)$ is the radial distribution function of atom X around the nitrogen atom of pyridazine. It can be seen that the coordination numbers of hydrogen are in good agreement with those obtained by the QM/MM results. As seen from the radial distribution functions, the coordination numbers of oxygen at short distances do not accord with the QM/MM results. However, these two curves match well at distances longer than 5 Å. This shows that the averaged effect from solvent molecules at larger distances is similar in both RISM-SCF-SEDD and QM/MM.

TABLE VI. The ^{15}N chemical shift of pyridazine relative to the gas-phase value. The results of the PCM and RISM-SCF-SEDD method were compared with the experimental values.[29]

	Water	Methanol	Acetone	$CHCl_3$	CCl_4
PCM	27.9	27.0	26.2	19.4	11.8
SEDD	54.5	32.9	16.1	6.5	0.3
Expt.[a]	51.8	39.3	19.7	26.6	16.2

[a]See Ref. 44.

We next investigated the ^{15}N chemical shift of pyridazine in various solvents. Based on the above results, we chose the cc-pVTZ basis set for the calculation. Other conditions were same as the previous calculation.

In Table VI, the chemical shifts with regard to the gas-phase value are shown. It can be seen that the value that is close to the experimental data is obtained with the RISM-SCF-SEDD calculation in water, methanol, and acetone, which are polar solvents. Based on these results, it can be said that the RISM-SCF-SEDD method properly describes the electrostatic interaction between the solute and the solvent, which leads to quantitative agreement. On the other hand, the values in chloroform and carbon tetrachloride are underestimated compared with the PCM results. This is because the interaction between the solute and the solvents was mainly non-electrostatic. To solve this problem, another approach that describes solute–solvent interactions at a higher level[85,86] may be necessary. It should be noted that the shifts in the group of polar and non-polar solvents qualitatively match the experimental results (water > methanol > acetone and chloroform > carbon tetrachloride).

IV. CONCLUSION

In this paper, we developed a new method for calculating the nuclear magnetic shielding tensor combined with the RISM-SCF-SEDD method. Although the approach combining the conventional RISM-SCF method with NMR calculation was carried out,[57,58] the description of the electrostatic interaction was insufficient, and the application was limited because of numerical instability. The present method removed these difficulties and extended its applicability to various systems.

We showed that a similar formalism to the previous study[57,58] can be applied for NMR calculation when using RISM-SCF-SEDD.

We implemented this new method and then examined the two systems as application examples. One is the basic and small molecule, H_2O. We ensured that our method is consistent with the previous results that the proton chemical shifts become close to the gas-phase value when the temperature increases. It is also confirmed that the proton chemical shifts of a water molecule were seen in the lower magnetic field region in the order of water, acetone, chloroform, and carbon tetrachloride. We obtained more accurate results for chemical shifts in polar solvents compared to the original RISM-SCF work.[58]

Next, we demonstrated the results of calculating ^{15}N chemical shifts of pyridazine and pyrazine. We first examined the basis set dependence of NMR calculation and confirmed that the results were systematically improved when using a larger basis set. Our new method gave considerably good results for azines in water compared with the PCM results. The reason why our method can obtain quantitative chemical shifts is the proper description of the electrostatic interaction, which was demonstrated in two RDFs. The advantage of our method is to obtain statistically converged results at only one calculation, and it is believed that this method can be widely applicable. On the other hand, in the solvent in which non-electrostatic interaction was dominant, good results were not obtained. In our future work, we will incorporate such interactions into the theoretical framework. As a further extension, there is also possibility to adopt a newly devised method for determining electron density with the constraint condition[87,88] in order to further expand the applicability of the present framework toward more diverse molecular species.

ACKNOWLEDGMENTS

This work was supported by JSPS KAKENHI (Grant Nos. JP17H03009 and JP18H04657). Theoretical computations were partly performed using Research Center for Computational Science, Okazaki, Japan.

APPENDIX A: DERIVATION OF EQ. (23)

Here, the detail of deriving Eq. (23) is shown. The derivative of Helmholtz free energy with respect to m_β^X is[61]

$$
\begin{aligned}
\frac{\partial A}{\partial m_\beta^X} &= \frac{\partial E_{\text{solute}}}{\partial m_\beta^X} + \frac{\partial \Delta\mu}{\partial m_\beta^X} \\
&= \frac{\partial}{\partial m_\beta^X}\sum_{\mu\nu} P_{\mu\nu}\left(H_{\mu\nu} + \frac{1}{2}\sum_{\rho\sigma} P_{\rho\sigma} G_{\mu\nu\rho\sigma}\right) + \frac{\partial}{\partial m_\beta^X}\left(-\frac{1}{\beta}\right)\sum_{\gamma s}\rho_s \int d\mathbf{r}\left[e^{-\beta u_{\gamma s}(r)+t_{\gamma s}(r)} - 1 - t_{\gamma s}(r) + \frac{1}{2}h_{\gamma s}^2(r) - h_{\gamma s}(r)t_{\gamma s}(r)\right] \\
&\quad + \frac{\partial}{\partial m_\beta^X}\left[\frac{1}{\beta}\int d\mathbf{r}\sum_{\gamma s}\rho_s h_{\gamma s}(r)c_{\gamma s}(r) - \frac{1}{2\beta(2\pi)^3}\int d\mathbf{k}\sum_{\gamma\delta st}\rho_s \hat{c}_{\gamma s}(k)\hat{c}_{\delta t}(k)\hat{\chi}_{st}(k)\hat{\omega}_{\gamma\delta}(k)\right] \\
&= \sum_{\mu\nu}\frac{\partial P_{\mu\nu}}{\partial m_\beta^X}\left(H_{\mu\nu} + \sum_{\rho\sigma} P_{\rho\sigma} G_{\mu\nu\rho\sigma}\right) + \sum_{\mu\nu} P_{\mu\nu}\frac{\partial H_{\mu\nu}}{\partial m_\beta^X} - \frac{1}{\beta}\sum_{\gamma s}\rho_s \int d\mathbf{r}\left\{\left[e^{-\beta u_{\gamma s}(r)+t_{\gamma s}(r)} - 1 - h_{\gamma s}(r)\right]\frac{\partial t_{\gamma s}(r)}{\partial m_\beta^X} + \left[-t_{\gamma s}(r) + h_{\gamma s}(r) - c_{\gamma s}(r)\right]\frac{\partial h_{\gamma s}(r)}{\partial m_\beta^X}\right. \\
&\quad \left. + \left[-h_{\gamma s}(r) + \sum_{\delta t}\omega_{\gamma\delta} * c_{\delta s} * \chi_{st}(r)\right]\frac{\partial c_{\gamma s}(r)}{\partial m_\beta^X} - \beta e^{-\beta u_{\gamma s}(r)+t_{\gamma s}(r)}\frac{\partial u_{\gamma s}(r)}{\partial m_\beta^X}\right\} \\
&= \sum_{\mu\nu}\frac{\partial P_{\mu\nu}}{\partial m_\beta^X}\left(H_{\mu\nu} + \sum_{\rho\sigma} P_{\rho\sigma} G_{\mu\nu\rho\sigma}\right) + \sum_{\mu\nu} P_{\mu\nu}\frac{\partial H_{\mu\nu}}{\partial m_\beta^X} + \sum_{\gamma s}\rho_s \int d\mathbf{r}\, g_{\gamma s}(r)\left(-q_s\sum_{i\in\gamma}\frac{\partial d_i}{\partial m_\beta^X}\int d\mathbf{r}'\frac{f_i(\mathbf{r}')}{|\mathbf{r}-\mathbf{r}'|}\right) \\
&= \sum_{\mu\nu}\frac{\partial P_{\mu\nu}}{\partial m_\beta^X} F_{\mu\nu}^{\text{gas}} + \sum_{\mu\nu} P_{\mu\nu}\frac{\partial H_{\mu\nu}}{\partial m_\beta^X} - \sum_i V_i\frac{\partial d_i}{\partial m_\beta^X}.
\end{aligned}
\tag{A1}
$$

One can know that the terms with derivatives of t, h, and c with respect to m_β^X are zero by using RISM and HNC equations and the definition of t. In the deformation process of Eq. (A1), following relations are utilized:

$$
\begin{aligned}
\frac{\partial u_{\gamma s}(r)}{\partial m_\beta^X} &= \frac{\partial}{\partial m_\beta^X}\left(u_{\gamma s}^{\text{CL}}(r) + u_{\gamma s}^{\text{LJ}}(r)\right) \\
&= -q_s\sum_{i\in\gamma}\frac{\partial d_i}{\partial m_\beta^X}\int d\mathbf{r}'\frac{f_i(\mathbf{r}')}{|\mathbf{r}-\mathbf{r}'|},
\end{aligned}
\tag{A2}
$$

$$
\begin{aligned}
&\sum_{\gamma s}\rho_s \int d\mathbf{r}\, g_{\gamma s}(r)\left(-q_s\sum_{i\in\gamma}\frac{\partial d_i}{\partial m_\beta^X}\int d\mathbf{r}'\frac{f_i(\mathbf{r}')}{|\mathbf{r}-\mathbf{r}'|}\right) \\
&\quad = -\sum_i\sum_s \rho_s q_s \int d\mathbf{r}\,\{h_{\gamma s}(r)+1\}\int d\mathbf{r}'\frac{f_i(\mathbf{r}')}{|\mathbf{r}-\mathbf{r}'|}\frac{\partial d_i}{\partial m_\beta^X} \\
&\quad = -\sum_i V_i\frac{\partial d_i}{\partial m_\beta^X}.
\end{aligned}
\tag{A3}
$$

In Eq. (A3), the final expression is obtained because the sum of the solute charges is zero.

APPENDIX B: THE DERIVATIVE OF V_i WITH RESPECT TO B_α

In order to calculate the derivative of V_i with respect to B_α, the derivative of $h_{\gamma s}$ with respect to B_α is necessary. This is obtained by differentiating the HNC closure relationship,

$$\frac{\partial h_{\gamma s}(r)}{\partial B_\alpha} = (h_{\gamma s}(r)+1)\frac{\partial}{\partial B_\alpha}[-\beta u_{\gamma s}(r)+h_{\gamma s}(r)-c_{\gamma s}(r)]. \quad \text{(B1)}$$

We can write the components of $\mathbf{d}$ as

$$d_i = \sum_{\mu\nu} P_{\mu\nu}\langle\chi_\mu|b_i|\chi_\nu\rangle, \quad \text{(B2)}$$

where the components of operator $\mathbf{b}$ are

$$b_i(\mathbf{r}) = \int d\mathbf{r}' \sum_k X^{-1}_{ik}|\mathbf{r}-\mathbf{r}'|f_k(\mathbf{r}') + \frac{\sum_k X^{-1}_{ik}Z_k}{\mathbf{Z}^t X^{-1}\mathbf{Z}} \times\left\{1-\int d\mathbf{r}'\sum_{ml} Z_m X^{-1}_{ml}|\mathbf{r}-\mathbf{r}'|f_l(\mathbf{r}')\right\}. \quad \text{(B3)}$$

The derivative of d_i with respect to B_α at zero field is

$$\begin{aligned}\left.\frac{\partial d_i}{\partial B_\alpha}\right|_{\mathbf{B}=\mathbf{0}} &= \sum_{\mu\nu}(P^{(1,0)}_{\mu\nu})_\alpha\langle\phi_\mu|b_i|\phi_\nu\rangle \\ &\quad + \sum_{\mu\nu}P^{(0)}_{\mu\nu}\left(\left\langle\frac{\partial\chi_\mu}{\partial B_\alpha}|b_i|\chi_\nu\right\rangle + \left\langle\chi_\mu|b_i|\frac{\partial\chi_\nu}{\partial B_\alpha}\right\rangle\right)\Big|_{\mathbf{B}=\mathbf{0}} \\ &= \sum_{\mu\nu}(P^{(1,0)}_{\mu\nu})_\alpha\langle\phi_\mu|b_i|\phi_\nu\rangle + \sum_{\mu\nu}P^{(0)}_{\mu\nu}Q_{\mu\nu}. \end{aligned} \quad \text{(B4)}$$

It is noted that these two matrices are skew-symmetric,

$$(P^{(1,0)}_{\mu\nu})_\alpha = -(P^{(1,0)}_{\nu\mu})_\alpha, \quad \text{(B5)}$$

$$Q_{\mu\nu} = -Q_{\nu\mu}. \quad \text{(B6)}$$

The trace of the product of a symmetric and a skew-symmetric matrix is zero, and this concludes

$$\left.\frac{\partial d_i}{\partial B_\alpha}\right|_{\mathbf{B}=\mathbf{0}} = 0. \quad \text{(B7)}$$

By inserting this into Eq. (B1), one can know that one of the solutions which is consistent with the derivative of the RISM equation

$$\left.\frac{\partial h_{\gamma s}(r)}{\partial B_\alpha}\right|_{\mathbf{B}=\mathbf{0}} = \sum_{\delta t}\omega_{\gamma\delta} * \left.\frac{\partial c_{\delta t}}{\partial B_\alpha}\right|_{\mathbf{B}=\mathbf{0}} * \chi_{ts}(r), \quad \text{(B8)}$$

is given as

$$\left.\frac{\partial h_{\gamma s}(r)}{\partial B_\alpha}\right|_{\mathbf{B}=\mathbf{0}} = \left.\frac{\partial c_{\gamma s}(r)}{\partial B_\alpha}\right|_{\mathbf{B}=\mathbf{0}} = 0 \quad (\text{for all } \gamma, s), \quad \text{(B9)}$$

and thus, the derivative of V_i with respect to B_α vanishes,

$$\left.\frac{\partial V_i}{\partial B_\alpha}\right|_{\mathbf{B}=\mathbf{0}} = 0. \quad \text{(B10)}$$

REFERENCES

[1] J. M. Seco, E. Quiñoá, and R. Riguera, Chem. Rev. **104**, 17 (2004).
[2] E. E. Kwan and S. G. Huang, Eur. J. Org. Chem. **2008**, 2671.
[3] J. M. Seco, E. Quiñoá, and R. Riguera, Chem. Rev. **112**, 4603 (2012).
[4] Z. Xu, C. Liu, S. Zhao, S. Chen, and Y. Zhao, Chem. Rev. **119**, 195 (2018).
[5] N. Bross-Walch, T. Kühn, D. Moskau, and O. Zerbe, Chem. Biodiversity **2**, 147 (2005).
[6] A. Cavalli, X. Salvatella, C. M. Dobson, and M. Vendruscolo, Proc. Natl. Acad. Sci. U. S. A. **104**, 9615 (2007).
[7] I. R. Kleckner and M. P. Foster, Biochim. Biophys. Acta, Proteins Proteomics **1814**, 942 (2011).
[8] M. Kovermann, P. Rogne, and M. Wolf-Watz, Q. Rev. Biophys. **49**, e6 (2016).
[9] A. Pastor and E. Martínez-Viviente, Coord. Chem. Rev. **252**, 2314 (2008).
[10] Y. Cohen and S. Slovak, Org. Chem. Front. **6**, 1705 (2019).
[11] M. W. Lodewyk, M. R. Siebert, and D. J. Tantillo, Chem. Rev. **112**, 1839 (2012).
[12] F. V. Toukach and V. P. Ananikov, Chem. Soc. Rev. **42**, 8376 (2013).
[13] M. Bühl and T. van Mourik, Wiley Interdiscip. Rev.: Comput. Mol. Sci. **1**, 634 (2011).
[14] D. Xin *et al.*, J. Org. Chem. **82**, 5135 (2017).
[15] T. Helgaker *et al.*, Chem. Rev. **112**, 543 (2012).
[16] E. E. Kwan and R. Y. Liu, J. Chem. Theory Comput. **11**, 5083 (2015).
[17] G. Saielli, Adv. Theory Simul. **1**, 1800084 (2018).
[18] J. Tomasi, B. Mennucci, and R. Cammi, Chem. Rev. **105**, 2999 (2005).
[19] B. Mennucci, Wiley Interdiscip. Rev.: Comput. Mol. Sci. **2**, 386 (2012).
[20] A. Bagno, F. Rastrelli, and G. Saielli, Chem. - Eur. J. **12**, 5514 (2006).
[21] R. Jain, T. Bally, and P. R. Rablen, J. Org. Lett. **74**, 4017 (2009).
[22] B. Mennucci, J. M. Martínez, and J. Tomasi, J. Phys. Chem. A **105**, 7287 (2001).
[23] B. Mennucci, J. Am. Chem. Soc. **124**, 1506 (2002).
[24] J. Tomasi, R. Cammi, B. Mennucci, C. Cappelli, and S. Corni, Phys. Chem. Chem. Phys. **4**, 5697 (2002).
[25] R. A. Klein, B. Mennucci, and J. Tomasi, J. Phys. Chem. A **108**, 5851 (2004).
[26] K. Aidas *et al.*, J. Phys. Chem. A **111**, 4199 (2007).
[27] R. M. Gester, H. C. Georg, S. Canuto, M. C. Caputo, and P. F. Provasi, J. Phys. Chem. A **113**, 14936 (2009).
[28] M. Dračínský and P. Bouř, J. Chem. Theory Comput. **6**, 288 (2010).
[29] V. A. Semenov, D. O. Samultsev, and L. B. Krivdin, Magn. Reson. Chem. **52**, 686 (2014).
[30] M. C. Caputo, P. F. Provasi, and S. P. Sauer, Theor. Chem. Acc. **137**, 88 (2018).
[31] Y. Y. Rusakov *et al.*, J. Phys. Chem. A **122**, 6746 (2018).
[32] A. Warshel and M. Levitt, J. Mol. Biol. **103**, 227 (1976).
[33] Q. Cui and M. Karplus, J. Phys. Chem. B **104**, 3721 (2000).
[34] J. Kongsted, A. Osted, K. V. Mikkelsen, and O. Christiansen, J. Phys. Chem. A **107**, 2578 (2003).
[35] D. Sebastiani and U. Rothlisberger, J. Phys. Chem. B **108**, 2807 (2004).
[36] B. Wang and K. M. Merz, J. Chem. Theory Comput. **2**, 209 (2006).
[37] A. H. Steindal, K. Ruud, L. Frediani, K. Aidas, and J. Kongsted, J. Phys. Chem. B **115**, 3027 (2011).
[38] V. Manzoni, M. L. Lyra, R. M. Gester, K. Coutinho, and S. Canuto, Phys. Chem. Chem. Phys. **12**, 14023 (2010).
[39] C. Steinmann, J. M. H. Olsen, and J. Kongsted, J. Chem. Theory Comput. **10**, 981 (2014).
[40] U. N. Morzan *et al.*, Chem. Rev. **118**, 4071 (2018).
[41] S. Komin, C. Gossens, I. Tavernelli, U. Rothlisberger, and D. Sebastiani, J. Phys. Chem. B **111**, 5225 (2007).
[42] J. Kongsted, C. B. Nielsen, K. V. Mikkelsen, O. Christiansen, and K. Ruud, J. Chem. Phys. **126**, 034510 (2007).
[43] J. Kongsted and B. Mennucci, J. Phys. Chem. A **111**, 9890 (2007).
[44] V. Manzoni, M. L. Lyra, K. Coutinho, and S. Canuto, J. Chem. Phys. **135**, 144103 (2011).
[45] D. Flaig, M. Beer, and C. Ochsenfeld, J. Chem. Theory Comput. **8**, 2260 (2012).
[46] S. Ten-no, F. Hirata, and S. Kato, J. Chem. Phys. **100**, 7443 (1994).

[47]H. Sato, F. Hirata, and S. Kato, J. Chem. Phys. **105**, 1546 (1996).
[48]H. Sato, Phys. Chem. Chem. Phys. **15**, 7450 (2013).
[49]E. L. Ratkova, D. S. Palmer, and M. V. Fedorov, Chem. Rev. **115**, 6312 (2015).
[50]D. Chandler and H. C. Andersen, J. Chem. Phys. **57**, 1930 (1972).
[51]F. Hirata and P. J. Rossky, Chem. Phys. Lett. **83**, 329 (1981).
[52]F. Hirata, *Molecular Theory of Solvation* (Springer Science & Business Media, 2003), Vol. 24.
[53]N. Minezawa and S. Kato, J. Phys. Chem. A **109**, 5445 (2005).
[54]M. Higashi and S. Kato, J. Phys. Chem. A **109**, 9867 (2005).
[55]T. Mori and S. Kato, Chem. Phys. Lett. **437**, 159 (2007).
[56]Y. Tanaka, N. Yoshida, and H. Nakano, Chem. Phys. Lett. **583**, 69 (2013).
[57]T. Yamazaki, H. Sato, and F. Hirata, Chem. Phys. Lett. **325**, 668 (2000).
[58]T. Yamazaki, H. Sato, and F. Hirata, J. Chem. Phys. **115**, 8949 (2001).
[59]A. Morita and S. Kato, J. Phys. Chem. A **106**, 3909 (2002).
[60]D. Yokogawa, H. Sato, and S. Sakaki, J. Chem. Phys. **126**, 244504 (2007).
[61]D. Yokogawa, H. Sato, and S. Sakaki, J. Chem. Phys. **131**, 214504 (2009).
[62]D. Yokogawa, K. Ono, H. Sato, and S. Sakaki, Dalton Trans. **40**, 11125 (2011).
[63]K. Iida and H. Sato, J. Phys. Chem. B **116**, 2244 (2012).
[64]S. Hayaki, Y. Kimura, and H. Sato, J. Phys. Chem. B **117**, 6759 (2013).
[65]Y. Matsumura, K. Iida, and H. Sato, Chem. Phys. Lett. **584**, 103 (2013).
[66]H. Nakano, J. Noguchi, T. Mochida, and H. Sato, J. Phys. Chem. A **119**, 5181 (2015).
[67]K. Kasahara, H. Nakano, and H. Sato, J. Phys. Chem. B **121**, 5293 (2017).
[68]K. Hirano, H. Nakano, Y. Nakao, H. Sato, and S. Sakaki, J. Comput. Chem. **38**, 1567 (2017).
[69]R. Ditchfield, Mol. Phys. **27**, 789 (1974).
[70]T. Helgaker and P. Jørgensen, J. Chem. Phys. **95**, 2595 (1991).
[71]S. J. Singer and D. Chandler, Mol. Phys. **55**, 621 (1985).
[72]R. Ahlrichs, Phys. Chem. Chem. Phys. **8**, 3072 (2006).
[73]M. J. Frisch *et al.*, Gaussian 16 Revision A.03, Gaussian, Inc., Wallingford, CT, 2016.
[74]M. Nakahara and C. Wakai, Chem. Lett. **21**, 809 (1992).
[75]H. J. Berendsen, J. P. Postma, W. F. van Gunsteren, and J. Hermans, "Interaction models for water in relation to protein hydration," in *Intermolecular Forces* (Springer, 1981), pp. 331–342.
[76]W. L. Jorgensen, J. Chandrasekhar, J. D. Madura, R. W. Impey, and M. L. Klein, J. Chem. Phys. **79**, 926 (1983).
[77]H. Sato and F. Hirata, J. Chem. Phys. **111**, 8545 (1999).
[78]F. Hirata and R. M. Levy, Chem. Phys. Lett. **136**, 267 (1987).
[79]B. M. Pettitt and P. J. Rossky, J. Chem. Phys. **77**, 1451 (1982).
[80]W. L. Jorgensen, D. S. Maxwell, and J. Tirado-Rives, J. Am. Chem. Soc. **118**, 11225 (1996).
[81]R. E. Hoffman, Magn. Reson. Chem. **44**, 606 (2006).
[82]W. L. Jorgensen and N. A. McDonald, J. Mol. Struct.: THEOCHEM **424**, 145 (1998).
[83]J. Tomasi, B. Mennucci, and E. Cancès, J. Mol. Struct.: THEOCHEM **464**, 211 (1999).
[84]A. Rohatgi, WebPlotDigitizer, https://automeris.io/WebPlotDigitizer/, 2017.
[85]N. Yoshida and S. Kato, J. Chem. Phys. **113**, 4974 (2000).
[86]T. Yamazaki, H. Sato, and F. Hirata, J. Chem. Phys. **119**, 6663 (2003).
[87]D. Yokogawa, Chem. Phys. Lett. **587**, 113 (2013).
[88]D. Yokogawa, Bull. Chem. Soc. Jpn. **91**, 1540 (2018).